Snow Crash: Compaction craters on (486958) Arrokoth and other small KBOs

William B. McKinnon[1], Xiaochen Mao[1], P. M. Schenk[2], K. N. Singer[3], S. J. Robbins[3], O. L. White[4,5], R. A. Beyer[4,5], S. B. Porter[3], J. T. Keane[6], D. T. Britt[7], J. R. Spencer[3], W. M. Grundy[8,9], J. M. Moore[6], S. A. Stern[3], H. A. Weaver[10], and C. B. Olkin[3]

[1]Department of Earth and Planetary Sciences and McDonnell Center for the Space Sciences, Washington University in St. Louis, St. Louis, MO, USA

[2]Lunar and Planetary Institute, Houston, TX, USA

[3]Southwest Research Institute, Boulder, CO, USA

[4]SETI Institute, Mountain View, CA, USA

[5]Space Science Division, NASA Ames Research Center, Moffett Field, CA, USA

[6]Jet Propulsion Laboratory, California Institute of Technology, Pasadena, CA, USA

[7]Department of Physics, University of Central Florida, Orlando, FL, USA

[8]Lowell Observatory, Flagstaff, AZ, USA.

[9]Department of Astronomy and Planetary Science, Northern Arizona University, Flagstaff, AZ 86011, USA

[10]Space Department, Johns Hopkins University Applied Physics Laboratory, Laurel, MD, USA

Corresponding author: William B. McKinnon (mckinnon@wustl.edu)

Word count for PU: 4000

Number of figures: 4

Key points

- Arrokoth is likely a low density, highly porous, contact binary planetesimal
- Impact craters on Arrokoth, and particularly its largest, likely formed as compaction craters, with modest or little ejecta
- High porosity acted to protect Arrokoth from catastrophic disruption, ejecta recoil, and lobe dislocation and rearrangement

Abstract

Evidence from Arrokoth and comets strongly suggests a very low density for this and similar small Kuiper belt objects. Plausible compositions imply very high porosities, in excess of 70%, and low compaction crush strengths. If so, craters on Arrokoth (especially Sky, its largest) formed largely by compaction of pore space and material displacement. This is consistent with geological evidence from *New Horizons* imaging. High porosity reduces cratering efficiency in the gravity regime whereas compaction moves it towards a crush strength scaling. Compaction also guarantees that most impactor kinetic energy is taken up as waste heat near the impact point, with momentum transferred to the rest of the body by elastic waves only. Monte Carlo simulations of Sky-forming conditions indicate that the momentum imparted likely separated Arrokoth's two lobes, but displacement was limited by dissipation at the neck. Unusual strength properties are not required to preserve Arrokoth's bilobate configuration.

Plain Language Summary

It has become apparent over the last few years that small asteroids and comets are very underdense compared with the materials they are made of. This means that their total porosities are likely quite high, in excess of 70%, both as tiny voids within particles (so-called microscopic porosity) and spaces between particles (macroscopic porosity). But none are likely as porous as the distant denizens of the Kuiper belt such as Arrokoth (visited by the *New Horizons* spacecraft in 2019). This paper concerns impact craters on Arrokoth and similar small bodies, and the rather unusual effects expected. Imagine a fluffy (fine powder) snowball striking a much larger fluffy snowball, only that the snow is not pure ice but a mixture of porous icy, rocky, and carbon-rich particles. Even at high velocities (>100s of meters/sec) craters should mostly form by compacting pore space and pushing material away from the impact point, not the traditional blasting of ejecta back into space. Similar to crush-up of an automobile bumper, compaction protects from the potentially catastrophic effects of large impacts, such as complete disruption of the target or breakup of bilobate bodies like Arrokoth, and should be incorporated in future collisional evolution studies.

1. Introduction

The slow spin of cold classical Kuiper belt object (CCKBO) Arrokoth (formerly 2014 MU_{69}) as well as its gravitational surface slope distribution and structural integrity suggest it is a remarkably low-density body, ~250-500 kg m^{-3} (Stern et al., 2019; Spencer et al., 2020; McKinnon et al., 2020; Keane et al., 2020; Hirabayashi et al., 2020; Mao et al., 2021). Such a density is at the lower end of estimates for cometary nuclei (with which Arrokoth likely shares a similar formation history; Nesvorný, 2018; Morbidelli & Nesvorný, 2020), and is even lower than that of 67P/Churyumov-Gerasimenko (67P), 532 ± 7 kg m^{-3} (Groussin et al., 2019). A bulk density between 250 and 500 kg m^{-3} implies substantial porosity (>70%) for both cometary and Arrokoth's presumed ice + refractory dust composition (Mumma and Charnley, 2011; Grundy et al., 2020). Such porosity extremes are not unknown in low pressure environments, where irregular particles are governed by weak frictional and cohesive contact forces, such as apply to relatively fresh, cold snow. Moreover, such porosities, and the low resistance to crushing (densification) pressure change the way a body responds to impacts, both in terms of cratering mechanics and globally (Collins et al., 2019). In this paper we discuss these possibilities in the context of Arrokoth's craters, and especially its largest, Sky (formerly "Maryland").

2. Density and Strengths of Arrokoth and Cometary Analogues

Comets are generally thought to be low-density based on non-gravitational force measurements (see Table 1 in Groussin et al., 2019), though systematic uncertainties are arguably underestimated (Peale, 1989). The density of 67P is of course well known from its in situ spacecraft mass determination (Pätzold et al., 2016). Physically rigorous limits on the density of another notable comet, Shoemaker-Levy 9 (SL9), were obtained by numerical simulations of its 1992 tidal breakup by Jupiter. Asphaug & Benz (1996) found that a progenitor nuclear density of ~600 kg m^{-3} best accounted for the formation of the "string of pearls" fragment chain. A later suite of n-body calculations, based on polyhedral rubble elements and frictional contact forces, implied an even lower density range for the SL9 progenitor, ~300-400 kg m^{-3} (Movshovitz et al., 2012).

Concerning CCKBOs, if Arrokoth's topography behaves similarly to that of asteroids and cometary nuclei (Richardson et al., 2015), the observed minimum in its mean gravitational slope (as a function of bulk density; see Fig. 3 in McKinnon et al., 2020) may signify a state of

maximum topographic stability and lowest internal stress, thus implying an approximate density (see Keane et al., 2020). This minimum, while broad, is centered near ρ = 240 kg m^{-3}. And 500 kg m^{-3} has been suggested as an upper limit to Arrokoth's bulk density, from the global stability of its contact binary configuration (Hirabayashi et al., 2020), though this was based on a simplified version of an early, less accurate shape model.

Present-day gravitational and rotational stresses on the contact or "neck" between Arrokoth's two lobes are a function of the body's bulk density ρ. Assuming the same value for both lobes, at ρ = 250 kg m^{-3} there is effectively zero contact stress, whereas common theoretical assumptions for the tensile strength (σ_t) and cohesion (c) of cometary materials (~100 Pa and 1 kPa, respectively; e.g., Jutzi et al., 2017) permit a wider range of densities (250-500 kg m^{-3}) to be supported; see Figure 2 in McKinnon et al. (2020). Geological estimates of cometary compressive strengths (σ_c), estimates from the lunar regolith, and laboratory measurements and modeling generally imply lower strengths than even these assumed values (Groussin et al., 2019), supporting the inference that Arrokoth is indeed very low density (i.e., $\rho <$ 500 kg m^{-3}).

Stresses at the fractured neck between the two lobes of 67P imply a $\sigma_c \sim$ 450 Pa (Matonti et al., 2019), which is a good limiting measure for the bulk, unconfined compressive strength of 67P (see also text S1). This value compares favorably with the minimum cohesion (c) estimates of ~100-400 Pa derived for over-steepened slopes on Arrokoth (near its neck) by McKinnon et al. (2020). Note that due to internal friction, σ_c exceeds c, but both are smaller than the stress required to crush out porosity, or crush strength Y_c, discussed next.

3. Porosity and Compaction Cratering

Because Arrokoth is likely not deficient in relatively involatile rocky and organic materials, i.e., is not simply icy (Grundy et al., 2020), the low densities above imply considerable porosity (both microscopic + macroscopic), likely well in excess of 50%. (And for comparison, Groussin et al. (2019) report a porosity estimate from CONSORT microwave sounding of ≈75-85% for the interior of 67P.) When the porosity of a surface is high enough (above the usual close packing thresholds for granular materials of 30-40%) and the crushing strength low enough, impact craters can form partially or wholly by compaction (Figure S2) as opposed to excavation and displacement (Housen et al., 2018; Collins et al., 2019). Arrokoth almost certainly meets the

porosity requirement. In Housen et al. (2018) crushing strength (Y_c) estimates were provided for a variety of porous asteroidal analogue materials (e.g., pumice, perlite), generally in excess of ~1 MPa (Y_c being defined as the pressure at which the original porosity is reduced by half). The transition to compaction cratering was determined experimentally to occur when $\rho g H \gtrsim 0.005 Y_c$, where g is surface gravity and H is crater depth. For Arrokoth, this should occur for

$$H \gtrsim 0.005\, Y_c/\rho g = 100 \text{ m} \times (Y_c/10 \text{ kPa}) \times (500 \text{ kg m}^{-3}/\rho)^2 \quad . \quad (1)$$

Limited experimental evidence shows that the Y_c for cold (77 K), granular ice (Durham et al., 2005) and porous ice-silicate mixtures (Yasui & Arakawa, 2009) are lower than those for silicaceous materials such as perlite at the same porosity (Figure S3), although no experiments have been carried out on ice-rock(-organic) mixtures at the large porosities (≳70%) nominally appropriate to Arrokoth. But even $Y_c \sim 25$–100 kPa (plausible from Figure S3) would bring the 7-km-wide, 1-km-deep Sky (Arrokoth's largest identified crater) to the compaction cratering threshold (depending on bulk density). At this threshold ejecta formation is suppressed by an order of magnitude compared with that in the gravity regime (see Fig. 17 in Housen et al., 2018). If bulk Arrokoth has the crush strength of fresh snow (<few kPa, see, e.g., Fig. 10 in Wang et al., 2021), the compaction threshold occurs at much smaller scales, so most of its identified craters (Spencer et al., 2020; Schenk et al., 2021) could also have formed by compaction (but see text S2).

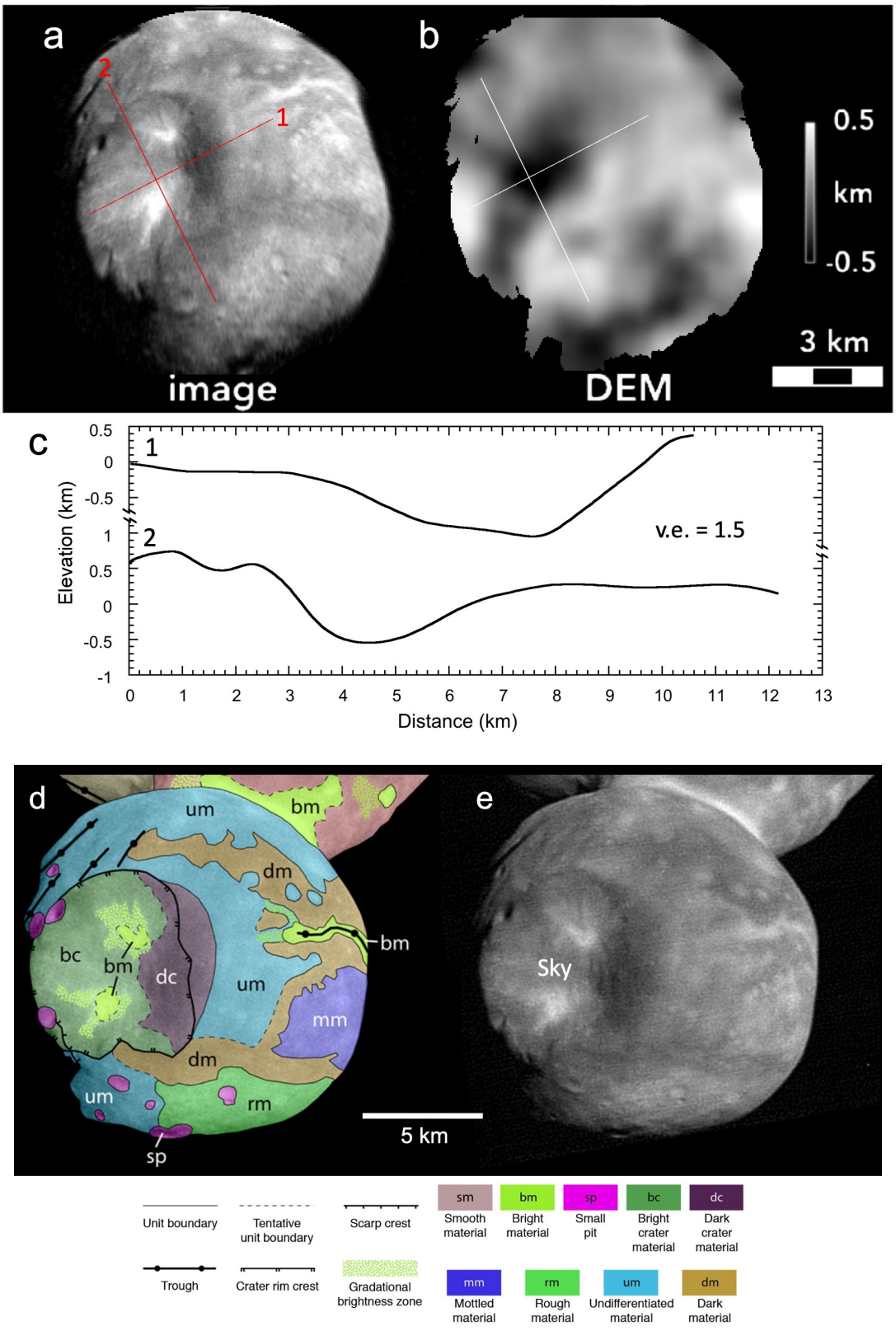

Figure 1. (a) Image and (b) stereogrammetric digital elevation model (DEM) of the Small Lobe (SL) of Arrokoth, with (c) representative topographic profiles below showing asymmetric shape

of the 7-km-wide crater Sky; note offset. The asymmetry is plausibly the result of oblique impact, which is accentuated for large impacts into convex shapes. Image and DEM are in orthographic projection centered on the visible disk of SL; updated from Schenk et al. (2021). (d) Geomorphological map of SL overlain on (e) portion of *New Horizons* observation CA06 (33 m/pixel). Units are labeled and colored as shown in the legend. Adapted from Spencer et al. (2020).

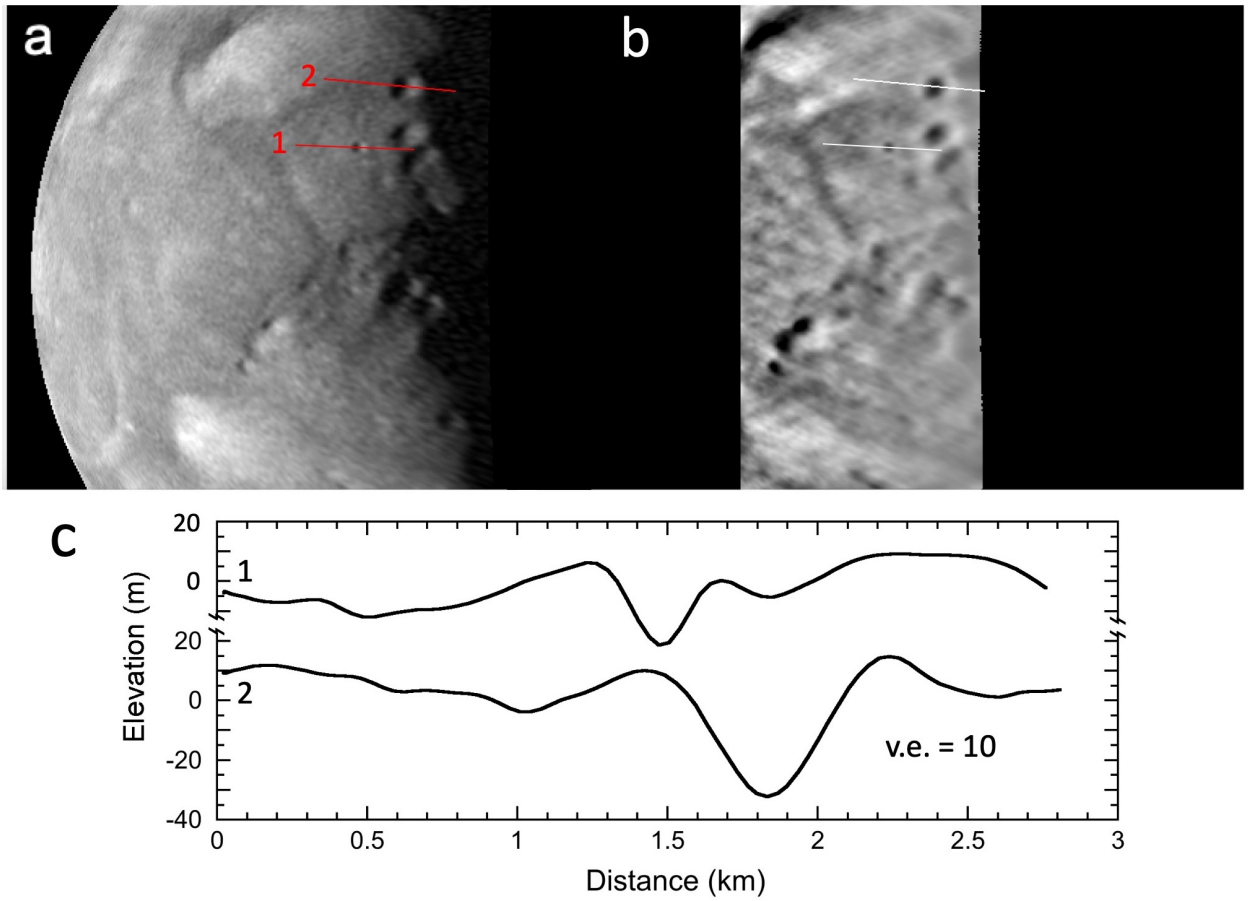

Figure 2. Topographic profiles across small (0.4 and 0.8 km) craters near the terminator of the Large Lobe (LL) on Arrokoth. Orthographic projection (a) and coincident photoclinometric DEM (b) centered on terminator region of LL, from Schenk et al. (2021). (c) The right-hand rim of crater 1 may be slightly elevated, or there may be an adjacent shallow topographic depression. Other small craters may lack rims simply due to great age and mass wasting.

4. Geological Evidence

It is notable that no evidence of a raised rim can be seen for Sky, although a slight one (≲50–75 m high) would not have been resolvable in the DEM (Schenk et al., 2021). This and its rounded

conical shape (Figure 1a-c) are consistent with the morphology of compaction craters formed in the laboratory (Housen & Holsapple, 2003; Housen et al., 2018). Nor are there albedo or morphological indications of an ejecta deposit in detailed mapping (Figure 1d). None of the other smaller craters on Arrokoth appear to possess rays or other ejecta patterns, though a couple have slightly raised rims (Figure 2). From these inferences, we suggest that crater formation on Arrokoth, at least at the scales resolvable by *New Horizons*, may have been dominated by displacement and compaction and not displacement and ejection, making Sky on Arrokoth more akin to Karoo (e.g.) on Mathilde (cf. Housen et al., 1999).

5. Implications

5.1. Spin Dynamics

In the compaction regime, crater size is a fixed ratio to impactor size, for constant impact velocity U and crush strength Y_c (Housen et al., 2018). Thus, there is nominally an opportunity to extract a measure of the impactor population's size-frequency distribution directly from crater counts. The retention of ejecta makes spin and other dynamical evolution modeling easier, as well, as collisions can be treated as completely inelastic, without recoil. For example, previously we (Mao et al., 2021) studied the spin evolution of Arrokoth under its bombardment history in the cold classical region of the Kuiper belt. We treated ejecta escape explicitly for each impact in a Monte Carlo model using standard ejecta scaling for a modestly porous granular target (i.e., a sand-like porosity closer to ~30-40%; Housen & Holsapple, 2011).

If we instead simply assume compaction cratering (for a highly porous target) in the limit in which all ejecta is retained (and thus angular momentum changes are a matter of simple vector addition), our results are modified as shown in Figure S4. The differences between Figure S4a and the results of the model simulations in Mao et al. (2021) are not significant in terms of final spin distributions. However, because ejecta are effectively suppressed in the compaction regime, it simplifies modeling of cratering using Arrokoth's true, complicated bilobate shape. Also, because compaction cratering is less efficient (discussed below), this increases the probability that an originally faster, synchronously spinning Arrokoth could have been slowed to its present spin period by impacts, or is at least not ruled out at the 3σ level, as long as its bulk density is $\lesssim$400 kg m^{-3} (Figure S4b).

Hereon we adopt the crater scaling of Housen et al. (2018) for *highly porous* granular materials (those with porosities n greater than 50%), their equation 20:

$$\pi_V = \left[0.75\left(\frac{Y_c}{\rho U^2}\right)^{-3\mu/2} + 0.023\,\pi_2^{-3\mu/(2+\mu)}\right] \times \mathrm{psf}(n) \quad , \qquad (2)$$

where $\pi_V \equiv \rho V/m$ is the cratering efficiency and $\pi_2 \equiv ga/U^2$ is the gravity-scaled size, with a and m the impactor radius and mass, respectively, and V the resulting crater volume (and where we have implicitly assumed equal densities for impactor and target). The exponent μ is 0.54, and psf(n) = 10.4*exp*(-5.07n) is an empirical porosity scale factor derived by Housen et al. (2018) from centrifuge impact experiments. For Arrokoth we assume that n increases linearly from 0.70 to 0.85 as bulk density decreases from 500 to 250 kg m^{-3}, and further adopt Y_c = 100 kPa, low enough so that compaction scaling is achieved for Sky, and consistent with experimental values for highly porous materials (see Figure S5). The greatest effects of compaction cratering on Arrokoth relate to the formation of Sky, given its potentially outsize effects on Arrokoth's spin state and structural stability, detailed below.

5.2. Small KBO SFD Controversy

The size-frequency distribution (SFD) for smaller KBO craters was measured directly on the unsaturated, ideally illuminated Charon cryovolcanic surface "Vulcan" Planitia (VP). Least-squares fits and maximum likelihood estimates (MLE) in Singer et al. (2019) gave shallow differential power-law slopes q near –1.7 or –1.8; MLE on VP craters mapped separately by S. Robbins gave slightly steeper slopes near –2.0, though –1.8 is preferred (as reported in Robbins & Singer, 2021) (and both papers quote slope uncertainties of 0.2-0.3; see Table 1 and Fig. 4 in the latter). These variations illustrate that fitting power-law slopes to modest numbers of craters (~100-200) yields results sensitive to fitting procedure, limits of completeness, etc. (see text S3). In contrast, Morbidelli et al. (2021) (M21) present a series of arguments based on less definitive Arrokoth crater data that the VP crater q is between –2.2 and –2.5, despite the incompatibility of such steeper slopes with the visible VP impact population.

The discrepancy is worse, however, when crater scaling is accounted for. For Charon the crater SFD implies an even *shallower* differential *impactor* SFD (Singer et al., 2021). For a more-or-less solid cryovolcanic surface and gravity scaling (Housen & Holsapple, 2011), the power-law slopes q of -1.7/-1.8/-2.0 above translate to impactor differential slopes q_i of -1.3/-1.4/-1.6 for

simple craters (-1.5/-1.6/-1.8 if complex). In contrast, for compaction scaling on Arrokoth q_i should be much closer to q, i.e., π_V is less dependent on π_2 (Figure S5), accentuating the fundamental q_i disagreement of Singer et al. (2019) and Robbins & Singer (2021)with M21 (who invoked traditional gravity scaling for Arrokoth's craters). Robbins et al. (2021), in a separate study, find that a shallow differential crater SFD of -1.66 ± 0.3 *is* compatible with Arrokoth's cratering record, in that formation of a singular, large crater (Sky) as an outlier is statistically admissible. We also note that VP is by definition a resurfaced unit and while ancient (Moore & McKinnon, 2021), it may not be quite as old a counting surface as Arrokoth, i.e., may not reflect the high, post-instability bombardment advocated by M21 to dominate Arrokoth (part of their chain of argument). It may also simply be that the impact crater population on Arrokoth, which is significantly less well characterized than VP's (Spencer et al., 2020; Schenk et al., 2021), offers greater latitude in interpretation than presented in M21.

5.3. Surface Densification and Heating.

Compaction (crush-up) implies that most of a given impactor's kinetic energy is taken up as waste heat below the impact point, with momentum transferred to the rest of the body by elastic waves (Collins et al., 2019). For typical CCKBO encounter velocities, impactor and near-field target temperatures should reach ~100 K, warm enough to mobilize hypervolatile ices, whereas faster, hot classical or scattered disk objects can melt methanol and water ice (see text S4). Stratigraphically, compaction craters consist of a densified lens buried by infilled loose surface material (Housen et al., 2018) (Figure S2). In contrast to a body like the Moon, where a volcanic surface can develop a fragmental surface layer or regolith under prolonged bombardment, a small underdense, granular KBO such as Arrokoth can thus develop a degree of armoring (at least subsurface) if sufficiently impacted.

Arrokoth's areal crater density is far from saturation (Spencer et al., 2021), but if there is a steeply increasing abundance of dust and other fine-scale debris in the Kuiper belt (see Fig. 5 in M21), then Arrokoth and other "pristine" CCKBO surfaces may actually be saturated by meter-scale impactors. Though below the resolution of *New Horizons* images, this may partially account, along with resolution and sun angle, for Arrokoth's smooth appearance (Figure 1).

5.4. Dust and Fragment Production

Because compaction cratering suppresses ejecta production, we suggest that much less KB ejecta

was produced by larger impacts on KBOs than if compaction is not common. Smaller cratering events, below the compaction size threshold (equation 1) would create escaping ejecta, however, which could act to populate the KBO dust complex (Poppe et al., 2019). The unusually shallow size-frequency distribution of smaller (~100-m to1-km) KBO impactors reflected in Charon and Pluto's craters (Singer et al., 2019; Robbins & Singer, 2021) may also be related, at least in part, to suppression of fragmentation during catastrophic impacts among highly porous bodies.

5.5. Contact Binary Stability

Compaction cratering is highly dissipative. For a highly porous body, crush up and near-field plastic deformation ("bumper effect") will limit far field damage to elastic reverberations, effectively shielding Arrokoth's SL (e.g.) from catastrophic disruption due to Sky's formation. Impactor momentum is not eliminated, but stability of the neck between the lobes requires careful consideration of the propagation of elastic waves in a highly porous medium.

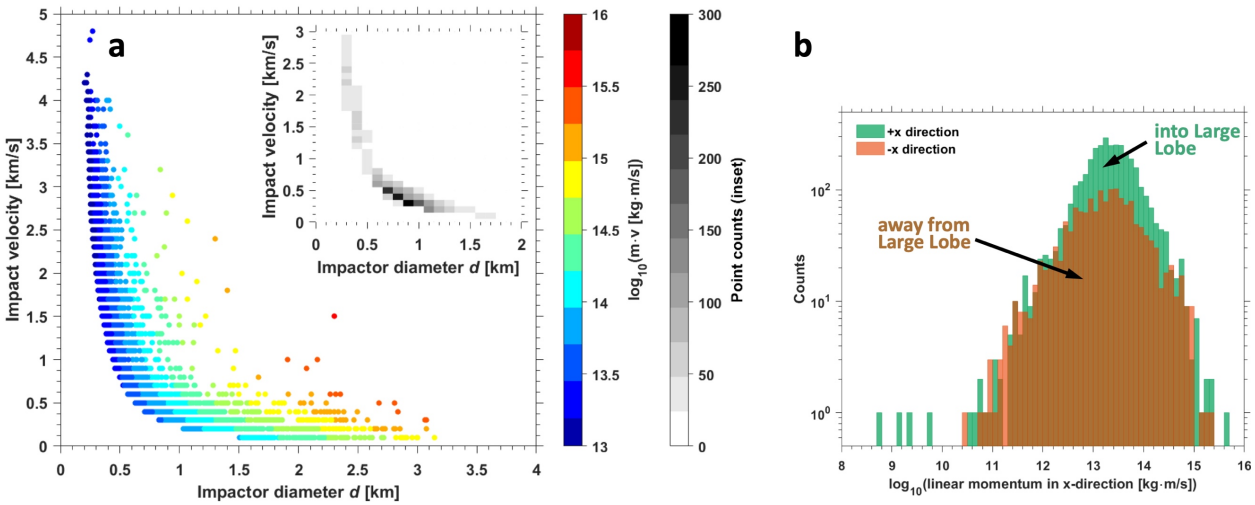

Figure 3. Monte Carlo distribution of impactor sizes and velocities that could have created Sky crater on Arrokoth. a) Color code indicates the linear momentum brought in by the impactor. Velocities are drawn from the distribution of impact speeds and diameters for small KBOs from Greenstreet et al. (2019); equal densities of 500 kg m^{-3} are assumed for impactor and target. Compaction crater scaling follows Equation 1 for $n = 0.7$ and $Y_c = 100$ kPa. Inset shows point count density of distribution. **b)** SL linear momentum component into and away from LL.

Figure 3 shows the results of a Monte Carlo simulation of the formation of Sky, for a

particular set of plausible compaction parameters (qualitatively similar results for other parameter combinations are shown in Figure S6). The most likely linear impactor momentum (Δp) imparted is close to $10^{13.75} \sim 5 \times 10^{13}$ kg m s^{-1}. The speed of the compressional wave that moves and reverberates across SL (and passes partially into the LL; Figure 4a) is uncertain. It depends both on the elastic moduli of Arrokoth's various constituents and how they are arranged, but mostly on the nature of the grain-to-grain contacts of what is almost certainly a very porous framework. For 67P, Knapmeyer et al. (2018) fit elastic wave data for snow as a function of density and predicted P-wave speeds of 1.7 km/s for snow of 500 kg m^{-3} density. But terrestrial snow is sintered and cemented, which is unlikely for small bodies like Arrokoth that have never experienced higher temperatures in bulk. Seismic wave speeds in dry quartz sand (shown in Goldreich & Sari [2009]) and determined for the lunar regolith (Larose et al., 2005) are much lower in comparison; here we adopt the P-wave speed for the upper few meters of lunar regolith (100 m s^{-1}; Cooper et al., 1974), as it is representative of the pressure conditions throughout the bulk of Arrokoth (the ratio of gravities is ~1000:1).

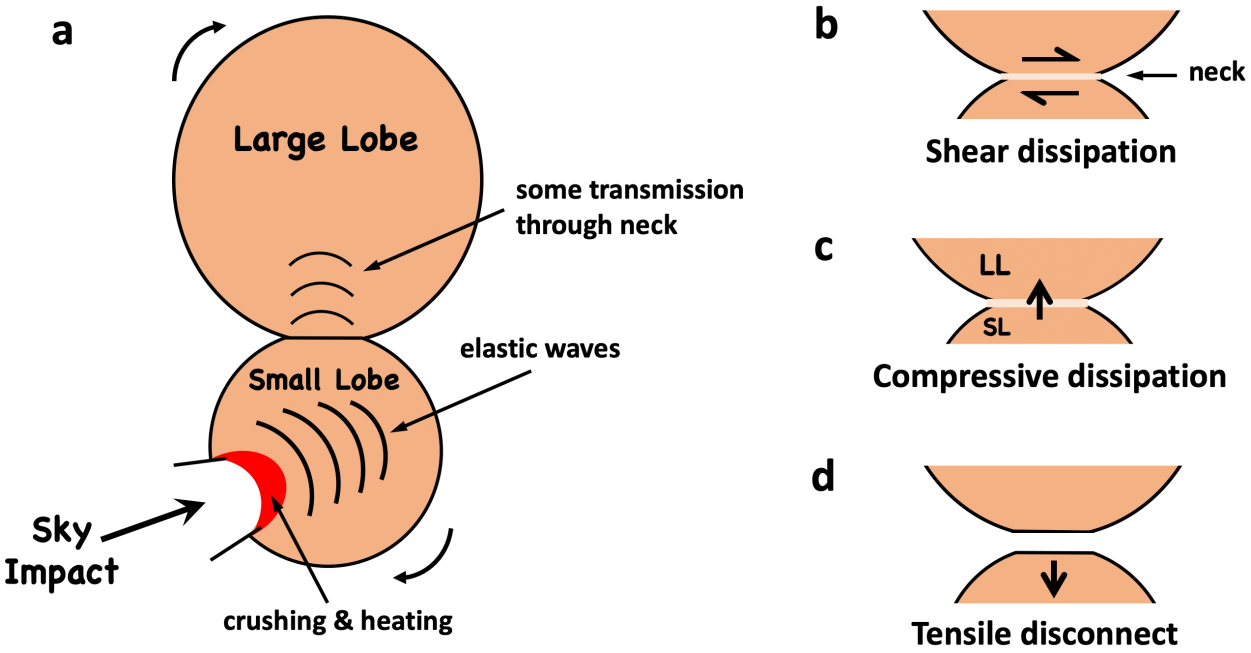

Figure 4. Schematic effects of Sky crater formation on Arrokoth. Presumed post lobe merger, the momentum imparted to SL is sufficient to disrupt the neck or join between the two lobes. End-member responses are shown at right, with some combination of shear and compressive dissipation limiting lobe motion at the neck being the most likely outcome (see text). Curved arrows at left indicate Arrokoth's pre-impact rotation.

From the shape of SL (Spencer et al., 2020), this wave speed gives an SL-crossing time (Δt) of ~150 sec, and a force $\Delta p/\Delta t \sim 4 \times 10^{11}$ N, which implies a resolved stress (shear+normal) on Arrokoth's ~23 km^2 neck area (McKinnon et al., 2020) of ~15 kPa. Greater than cometary strength estimates (Groussin et al. [2015] and earlier discussion), the implication is that the Sky impact most likely caused the neck or join between the two lobes to break (in agreement with Hirabayashi et al. [2020], though they derived generally higher neck stresses, principally because they adopted a much higher P-wave speed for Arrokoth).

Based on the SL mass for $\rho = 500$ kg m^{-3} and ellipsoidal dimensions in Spencer et al. (2020), the actual velocity impulse imparted to SL is only ~0.1 m s^{-1}, however, so it is not obvious that the lobes can actually completely separate. The kinetic energy of SL in this calculation, due to this motion, is 3×10^{12} J, a small fraction of the original kinetic energy brought in by the Sky impactor. The deformation at the neck, for most impactor trajectories, should have been some combination of crushing, compression, and shear; i.e., from the geometry of the impact, it is much more likely that SL is driven into LL than away (by a ratio of 3:1; Figure 3b). At minimum, the stresses in this case would be limited by Arrokoth's compressive and shear strengths (nominally 3 and 1 kPa, respectively, see Fig. 2 in McKinnon et al. [2020]). The work done would thus be ~1–3 kPa × 23 km^2 × l, where l is the displacement at the neck. We find that 3×10^{12} J can be dissipated at the neck by ~40-to-120 m of displacement, where the larger value refers to pure shear deformation (sliding) (see Figure 4b,c). Although these estimates are sensitive to impactor momentum, such modest or even larger offsets would not be discernable in available *New Horizons* imagery (we can't see into the neck region [Akasa Linea] at high resolution [Stern et al., 2021]; Figure 1e). More importantly, we predict that the Sky impact most likely did not lead to the complete lobe separation (in disagreement with Hirabayashi et al. [2020]).

The Sky impactor imparts both angular and linear momentum to SL. The distribution of angular momenta corresponding to the impacts in Figure 3 is shown in Figure S7. A typical value is ~$10^{17.3} = 2 \times 10^{17}$ kg m^2 s^{-1}, which for principal axis rotation corresponds to a tangential rotational velocity at the neck of ~0.1 m s^{-1} as well. Again, such velocity can be dissipated by shear friction at the neck over ~100 m of motion, as long as the 2 lobes remain in contact.

In the less likely case that the momentum impulse has an extensional component at the neck

(Figure 4d), the tensile strength at the neck is likely so low that the two lobes *would* separate. What happens next depends on how close Arrokoth is/was to its critical rotation period. For ρ = 500 kg m^{-3}, the two lobes are bound (Stern et al., 2019; McKinnon et al., 2020). For a gravitational potential energy between the two lobes of ~2 $\times 10^{15}$ J, 3 $\times$ 10^{12} J of kinetic energy is equivalent to an increase of ~20 m between the centers of mass of the two lobes, so the lobes in this case separate but recollide a few 100 sec later (if the gap does not get filled by sloughing loose surface material [Spencer et al., 2020; Stern et al., 2021]). But for densities near 250 kg m^{-3}, the two lobes are critically bound, so an outward radial impulse of 0.1 m s^{-1} would place the lobes into mutual orbit (with eccentricity ~0.1). Recollision would not occur until an orbital period later (16 hr), which would give (the rotating) SL time to shift or twist out of tidal alignment with LL. Because this does not appear to be case, we conclude that although this separation and orbital flight could have occurred, it did not.

6. Summary

The implications of compaction cratering for Arrokoth and other small KBOs are multiple: 1) impact ejecta and dust production is suppressed for the largest craters; 2) crater scaling depends on both porosity and a strength measure (Y_c); 3) crush up concentrates thermal effects near and below craters, potentially leading to surface devolatilization and armoring; 4) crush up protects small KBOs from catastrophic disruption; and 5) for Arrokoth and other contact binary KBOs, it stabilizes the join between lobes (e.g., we find the formation of Sky likely broke Arrokoth's neck, but it got better).

Acknowledgements

This research supported by NASA's *New Horizons* project.

Data Availability Statement

All manuscript data are publicly available through Figshare (Mao, 2022).

References

Asphaug, E., & Benz, W. (1996). Size, density, and structure of comet Shoemaker-Levy 9 inferred from the physics of tidal breakup. *Icarus*, *121*, 225–248. https://doi.org/10.1006/icar.1996.0083

Basilevsky, A. T., Krasil'nikov, S. S., Shiryaev, A. A., Mall, U., Keller, H. U., Skorov, Yu. V., et al. (2016). Estimating the strength of the nucleus material of comet 67P Churyumov–Gerasimenko. *Solar System Research*, *50*, 225–234. https://doi.org/10.1134/S0038094616040018

Collins, G. S., Housen, K. R., Jutzi, M., & Nakamura, A. M. (2019). Planetary impact processes in porous materials. In T. J. Vogler & D. A. Fredenburg (Eds.) *Shock Phenomena in Granular and Porous Materials* (pp. 103–136). Switzerland: Springer Nature. https://doi.org/10.1007/978-3-030-23002-9_4

Cooper, M. R., Kovach, R. L., & Watkins, J. S. (1974). Lunar near-surface structure. *Reviews of Geophysics and Space Physics*, *12*, 291–308. https://10.1029/RG012i003p00291

Durham, W. B., McKinnon, W. B., & Stern, L. A. (2005). Cold compaction of water ice. *Geophysical Research Letters*, *32*, L18202. https://doi.org/10.1029/2005GL023484

Goldreich, P., & Sari, R. (2009) *Astrophysical Journal*, *691*, 54–60.

Greenstreet, S., Gladman, B., McKinnon, W. B., Kavelaars, J. J., & Singer, K. N. (2019). Crater density predictions for New Horizons flyby target 2014 MU69. *Astrophys. J. Lett.*, *872*(1), L5. https://doi.org/doi:10.3847/2041-8213/ab01db

Groussin, O., Jorda, L., Auger, A.-T., Kührt, E., Gaskell, R., Capanna, C., et al. (2015). Gravitational slopes, geomorphology and material strengths of the nucleus of comet 67P/Churyumov-Gerasimenko from OSIRIS observations. *Astronomy & Astrophysics*, *583*, A32. https://doi.org/10.1051/0004-6361/201526379

Groussin, O., Attree, N., Brouet, Y., Ciarletti, V., Davidsson, B., Filacchione, G., et al. (2019). The thermal, mechanical, structural, and dielectric properties of cometary nuclei after Rosetta. *Space Science Reviews*, *215*, 29. https://doi.org/10.1007/s11214-019-0594-x

Grundy, W. M., Bird, M. K., Britt, D. T., Cook, J. C., Cruikshank, D. P., Howett, C. J. A., et al., (2020). Color, composition, and thermal environment of Kuiper Belt object (486958) Arrokoth. *Science*, *367*, eaay3705. https://doi.org/10.1126/science.aay3705

Hirabayashi, M., Trowbridge, A. J., & Bodewits, D. (2020). The mysterious location of Maryland on 2014 MU69 and the reconfiguration of its bilobate shape. *Astrophysics Journal Letters*, *891*, L12. https://doi.org/10.3847/2041-8213/ab3e74

Housen, K. R., & Holsapple, K.A. (2003). Impact cratering on porous asteroids. *Icarus*, *163*, 102–119. https://doi.org/10.1016/S0019-1035(03)00024-1

Housen, K. R., & Holsapple, K. A. (2011). Ejecta from impact craters. *Icarus*, *211*, 856-875. https://doi.org/10.1016/j.icarus.2010.09.017

Housen, K. R., Holsapple, K. A., & Voss, M. E. (1999). Compaction as the origin of the unusual craters on the asteroid Mathilde. *Nature*, *402*, 155–157. https://doi.org/10.1038/45985

Housen, K. R., Sweet, W. J., & Holsapple, K. A. (2018). Impacts into porous asteroids. Icarus 300**,** 72-96. https://doi.org/10.1016/j.icarus.2017.08.019

Jutzi, M., Benz, W., Toliou, A., Morbidelli, A., & Brasser, R. (2017). How primordial is the structure of comet 67P? Combined collisional and dynamical models suggest a late formation. *Astronomy & Astrophysics*, *597*, A61. https://doi.org/10.1051/0004-6361/201628963

Keane, J. T., Porter, S. B., Beyer, R. A., Umurhan, O. M., McKinnon, W. B., Moore, J. M., et al. (2020). Geophysics of (486958) Arrokoth revealed by New Horizons. *Bulletin of the American Astronomical Society, 52(6)*, abstract 508.02. https://baas.aas.org/pub/2020n6i508p02

Knapmeyer, M., Fischer, H.-H., Knollenberg, J., Seidensticker, K. J., Thiel, K., Arnold, W., et al. (2018). Structure and elastic parameters of the near surface of Abydos site on comet 67P/Churyumov–Gerasimenko, as obtained by SESAME/CASSE listening to the MUPUS insertion phase. *Icarus*, *310*, 165–193. https://doi.org/10.1016/j.icarus.2017.12.002

Larose, E., Khan, A., Nakamura, Y., & Campillo, M. (2005). Lunar subsurface investigated from correlation of seismic noise. *Geophysical Research Letters*, *32*, L16201, doi:10.1029/2005GL023518

Matonti, C. Attree, N., Groussin, O., Jorda, L., Viseur, S., Hviid, S. F., et al. (2019). Bilobate comet morphology and internal structure controlled by shear deformation. *Nature Geoscience*, *12*, 157–162. https://doi.org/10.1038/s41561-019-0307-9.

Mao, X. (2022). Simulation data for manuscript "Snow Crash: Compaction craters on (486958) Arrokoth and other small KBOs" [Data set]. Figshare. https://doi.org/10.6084/m9.figshare.19230135.v1.

Mao, X., McKinnon, W. B., Singer, K. N., Keane, J. T., Robbins, S. J., Schenk, P. M., et al. (2021). Merger and spindown of (486958) Arrokoth by collisions. *52nd Lunar and Planetary Science Conference*, abstract #2415. https://www.hou.usra.edu/meetings/lpsc2021/pdf/2415.pdf

McKinnon, W. B., Richardson, D. C., Marohnic, J. C., Keane, J. T., Grundy, W. M., Hamilton, D. P., et al. (2020). The solar nebula origin of (486958) Arrokoth, a primordial contact binary in the Kuiper Belt. *Science*, *367*, eaay6620. https://doi.org/10.1126/science.aay6620

Moore, J. M., & McKinnon, W. B. (2021). Geologically diverse Pluto and Charon: Implications for the dwarf planets of the Kuiper belt. *Annual Review of Eath and Planetary Sciences*, *49*, 173–200. https://doi.org/10.1146/annurev-earth-071720-051448

Morbidelli, A., & Nesvorný, D. (2020). Kuiper belt: formation and evolution. In D. Prialnik, M. A. Barucci, L. Young (Eds.), *The Trans-Neptunian Solar System* (pp. 25–59). Amsterdam: Elsevier. https://doi.org/10.1016/B978-0-12-816490-7.00002-3

Morbidelli, A., Nesvorný, D., Bottke, W. F., & Marchi, S. (2021). A re-assessment of the Kuiper belt size distribution for sub-kilometer objects, revealing collisional equilibrium at small sizes. *Icarus*, *356*, 114256. https://doi.org/10.1016/j.icarus.2020.114256

Movshovitz, N., Asphaug, E., & Korycansky, D. (2012). Numerical modeling of the disruption of comet D/1993 F2 Shoemaker-Levy 9 representing the progenitor by a gravitationally bound assemblage of randomly shaped polyhedral. *Astrophysical Journal*, *759*, 93. https://doi.org/10.1088/0004-637X/759/2/93

Mumma, M. J., & Charnley, S. B. (2011). The chemical composition of comets—Emerging taxonomies and natal heritage. *Annual Reviews of Astronomy and Astrophysics*, *49*, 471–524. https://10.1146/annurev-astro-081309-130811

Nesvorný, D. (2018). Dynamical evolution of the early Solar System. *Annual Review of Astronomy and Astrophysics*, *56*, 137–174. https://doi.org/10.1146/annurev-astro-081817-052028

O'Rourke, L., Heinisch, P., Blum, J., Fornasier, S., Filacchione, G., Van Hoang, H., et al. (2020). The Philae lander reveals low-strength primitive ice inside cometary boulders. *Nature*, *586*, 697–701. https://doi.org/10.1038/s41586-020-2834-3

Pajola, M., Vincent, J.-B., Güttler, C., Lee, J.-C., Bertini, I., Massironi, M., et al. (2015). Size-frequency distribution of boulders ≥7 m on comet 67P/Churyumov-Gerasimenko. *Astronomy & Astrophysics*, *583*, A37. https://doi.org/10.1051/0004-6361/201525975

Pätzold, M., Andert, T., Hahn, M., Asmar, S. W., Barriot, J.-P., Bird, M. K., et al. (2016). A homogeneous nucleus for comet 67P/Churyumov-Gerasimenko from its gravity field. *Nature*, *530*, 63–65. https://doi.org/10.1038/nature16535

Peale, S. J. (1989). On the density of Halley's comet. *Icarus*, *82*, 36–49. https://doi.org/10.1016/0019-1035(89)90021-3

Poppe, A. R., Lisse, C. M., Piquette, M., Zemcov, M., Horányi, M., James, D., et al. (2019). Constraining the solar System's debris disk with in situ *New Horizons* measurements from the Edgeworth-Kuiper Belt. *Astrophysics Journal Letters*, *881*, L12. https://doi.org/10.3847/2041-8213/ab322a

Richardson, J. E., Graves, K. J., Harris, A. W., & Bowling, T. J. (2019). Small body shapes and spins reveal a prevailing state of maximum topographic stability. *Icarus*, *329***,** 207–221. https://doi.org/10.1016/j.icarus.2019.03.027

Robbins S. J. & Singer, K. N. (2021) Pluto and Charon impact crater populations: Reconciling different results. *Planetary Science Journal*, *2*, 192. https://doi.org/10.3847/PSJ/ac0e94

Robbins, S. J., Riggs, J. D., & Parker, A. H. (2021). Is the diameter of Herschel crater, Mimas, an outlier? A mathematical framework for analyzing planetary feature size-frequency distribution anomalies. *Geophysical Research Letters*, *48*, e2021GL093247. https://doi.org/10.1029/2021GL093247

Schenk, P., Singer, K. N., Beyer, R., Beddingfield, C., Robbins, S. J., McKinnon, W. B., et al. (2021). Origins of pits and troughs and degradation on a small primitive planetesimal in the Kuiper Belt: high-resolution topography of (486958) Arrokoth (aka 2014 MU69) from New Horizons. *Icarus*, *356*, 113834. https://doi.org/10.1016/10.1016/j.icarus.2020.113834

Singer, K. N., McKinnon, W. B., Gladman, B., Greenstreet, S., Bierhaus, E. B., Stern, S. A., et al. (2019). Impact craters on Pluto and Charon indicate a deficit of small Kuiper belt objects. *Science*, *363*, 955–959. https://doi.org/10.1126/science.aap8628

Singer, K. N., Greenstreet, S., Schenk, P. M., Robbins, S. J., & Bray, V.J. (2021). Impact craters on Pluto and Charon and terrain age estimates**.** In S. A. Stern, J. M. Moore, W. M. Grundy, L. A. Young, & R. P. Binzel (Eds.) *Pluto System After New Horizons* (pp. 121–145). Tucson: University of Arizona Press. https://doi:10.2458/azu_uapress_9780816540945-ch007

Spencer, J. R., Stern, S. A., Moore, J. M., Weaver, H. A., Singer, K. N., Olkin, C. B., et al. (2020). The geology and geophysics of Kuiper Belt object (486958) Arrokoth. *Science*, *367*, aay3999. https://doi.org/10.1126/science.aay3999

Stern, S. A., Weaver, H. A., Spencer, J. R., Olkin, C. B., Gladstone, G. R., Grundy, W. M., et al. (2019). Initial results from the New Horizons exploration of 2014 MU69, a small Kuiper Belt object. *Science*, *364*, eaaw9771. https://doi.org/10.1126/science.aaw9771

Stern, S. A., Keeney, B., Singer, K. N., White, O., Hofgartner, J. D., Grundy, W., & the New Horizons Team (2021). Some new results and perspectives regarding the Kuiper belt object Arrokoth's remarkable, bright neck. *Planetary Science Journal*, *2*, 87, https://doi.org/10.3847/PSJ/abee26

Wang, E., Fu, X., Han, H., Liu, X., Xiao, Y., & Leng, Y. (2021). *Cold Regions Science and Technology*, *182*, 103215. https://doi.org/10.1016/j.coldregions.2020.103215

Yasui, M., & Arakawa, M. (2009). Compaction experiments on ice-silica particle mixtures: implications for residual porosity of small icy bodies. *Journal of Geophysical Research*, *114*, E09004. https://doi.org/10.1029/2009JE003374

References from the Supporting Information

Bakanova, A. A., Zubarev, V. N., Sutulov, Y.N., & Trunin, R. F. (1976). Thermodynamic properties of water at high pressures and temperatures, *Soviet Physics JETP, English Translation*, 41, 544– 548.

Cooper, M. R., Kovach, R. L., & Watkins, J. S. (1974). Lunar near-surface structure. *Reviews of Geophysics and Space Physics*, *12*, 291–308. https://10.1029/RG012i003p00291

Kieffer, S. W., & Simonds, C. H. (1980). The role of volatiles and lithology in the impact cratering process. *Reviews of Geophysics and Space Physics*, *18*, 143–181. https://10.1029/RG018i001p00143

McKinnon, W. B., Glein, C. R., Bertrand, T., & Rhoden, A. R. (2021). Formation, composition, and history of the Pluto system: A post-New Horizons synthesis. In S. A. Stern, J. M. Moore, W. M. Grundy, L. A. Young, & R. P. Binzel (Eds.) *The Pluto System After New Horizons* (pp. 507–543). Tucson: University of Arizona Press. https://doi:10.2458/azu_uapress_9780816540945-ch022

Stesky, R. M. (1978). Experimental compressional wave velocity measurements in compacting powders under high vacuum: applications to lunar crustal sounding. *Proceedings Lunar and Planetary Science Conference 9th*, 3637–3649. New York: Pergamon.